

Full Paper | <http://dx.doi.org/10.17807/orbital.v14i3.17429>

Experimental and Kinetic Study of the Effect of using Zr- and Pt-loaded Metals on Y-zeolite-based Catalyst to Improve the Products of *n*-heptane Hydroisomerization Reactions

Younus H. Khalaf* ^a, Bashir Y. Sherhan Al-Zaidi ^a, and Zaidoon M. Shakour ^a

The escalating cost of Pt metal has prompted researchers to incorporate other metals into Pt/catalysts to reduce the amount of Pt. In this work, several bimetallic Pt-Zr/HY-zeolite catalysts were prepared by incorporating small amounts of the inexpensive Zr into the Pt/HY-zeolite to form an active and selective catalyst. Results showed that although half of the required platinum metal was used, the catalytic activity of the prepared Pt-Zr/HY bimetallic catalyst was higher than that of the monometallic (Pt or Zr)/HY catalysts, as a result of the improved Lewis acidity of that catalyst that resulted from the addition of the Zr metal; additionally, the branched alkanes' yield also increased. The optimum catalyst was bimetallic, containing 0.5 wt% Pt + 0.5 wt% Zr, which achieved the highest yield of isomers at 70.2 mol%, along with 82.61 and 84.98 mol% for conversion and selectivity, respectively, under 1 MPa and 250°C reaction conditions. In addition, the hydroisomerization reaction kinetic model was achieved, giving good predicted results in agreement with the experimental calculations, with an acceptable relative error. It was found that lower activation energies (about 44.5 kJ/mol) were needed for olefin hydrogenation to iso-paraffins, while higher activation energies were required for *i*-paraffin hydrocracking (about 138.1 kJ/mol).

Graphical abstract



Keywords

Hydroisomerization process
Bimetallic Pt & Zr / Y-zeolite catalysts
Reaction kinetics of *n*-heptane

Article history

Received 24 Feb 2022
Revised 25 Jul 2022
Accepted 26 Jul 2022
Available online 30 Sep 2022

Handling Editor: Paulo de Sousa Filho

1. Introduction

Modern internal combustion engines (IC engines) with high compression ratios do not work appropriately unless high

octane gasoline is used, which is less likely to self-ignite when highly compressed, enabling the IC engines to perform high

^a Department of Chemical Engineering, University of Technology-Iraq, Alsinaa Street 52, 10066 Baghdad, Iraq. * Corresponding author. Email: che.19.22@grad.uotechnology.edu.iq; younus.khalaf@outlook.com

compression ratios, leading to more fuel consumption efficiency and the release of less carbon dioxide [1, 2]. According to the isomerization bifunctional mechanism proposed by Mills, high catalytic activity, selectivity, and stability can be attained only when using a catalyst that is composed of two components, metallic and acidic together, creating a bifunctional catalyst [3-6]. Noble metals supported on zeolites used in the hydroisomerization process provide the de/hydrogenation function. Furthermore, they can activate C-H, H-H, and C-C bonds and protect the catalyst surface from deactivation by preventing coke deposition with the help of hydrogen, maintaining the catalyst surface clean of heavy hydrocarbons [7, 8]. The percentages of metal dispersion loaded on the catalyst support, along with their particles exposed faces characteristics and metal-support interfaces, determine the overall catalytic properties [9]. However, if these metals particles were atomically dispersed through zeolite crystallites, their catalytic properties would be substantially different [10]. In this regard, these different metallic heteroatoms (i.e., Zr, Ti, Sn, Nb, Ta, and Hf) can be substituted as cation metals into the zeolite framework [11-14], conferring different physicochemical properties on the zeolite-based catalysts and significantly improving the catalytic features [8, 15]. In addition, incorporating these metals in tetrahedral coordination provides an extraordinary Lewis acidity to the zeolite-based catalyst, specifically, the Sn- and Zr-containing zeolites, which enables the preparation of very active and selective catalysts [16-19]. Different Lewis acidity strengths have been achieved by incorporating one of these heteroatoms metals into catalysts. Indeed, various researchers have theoretically assessed the Lewis acid strength order of the metals, concluding that the theoretical order of activity is as follows: $Zr > Sn > Pb > Ti > Si$ [20,21]. Earlier, Sinfelt had stated that incorporating another heteroatom metal with the noble metal Pt or Pd metal in the structure of the catalysts to compose the bimetallic catalyst would enhance the catalytic performance for hydroisomerization, including conversion, selectivity, and coke resistance [22-24]. This enhancement in catalytic features stems from the second metal acting as a promoter that modifies the metals' electronic and geometric structures inside the catalyst's body [8].

Many researchers have investigated the concept of bimetallic catalysts in preparing active, selective and stable catalysts, of which Yang et al. examined a novel bimetallic isomerization Pt-NiP/H β catalyst by introducing a small quantity of Pt into the NiP compound on the H β zeolite [25]. He found that this bimetallic catalyst demonstrated catalytic activity similar to Pt/H β and NiP/H β catalysts for the hydroisomerization of normal hexane. Kitaev et al. have investigated the bimetallic catalyst (0.2-0.8) wt% Zr-0.5 wt% Pt loaded on dealuminated zeolite Y. The acid properties and catalytic activity in n-hexane conversion were studied for dealuminated zeolite Y modified with zirconyl nitrate to yield zirconium. They have found that the zirconyl nitrate favors the formation of strong acid sites such that an increase in their relative amount leads to the enhancement of cracking activity in n-hexane conversion [26]. In addition, Jarvis et al. have explained that the addition of a second metal Zn to the catalyst Pt/ZSM5 increased selectivity towards the production of aromatics because of the increased formation of alkene intermediates; additionally, reforming n-octane with a bimetallic catalyst ZSM-5 loaded with Pt-Zn nanoparticles displayed a selectivity of over 90% for producing BTX and i-octane at 60% conversion with insignificant coke deposition [27]. Lin et al. has investigated the reforming of n-heptane by the bimetallic and trimetallic series of catalysts loaded on

chlorided alumina and ZSM5-zeolite; the bimetallic catalysts were composed of a supporter loaded with Pt and Sn, and the trimetallic catalysts were the bimetallic doped with cerium [28]. The researchers found that it could enhance the bimetallic catalyst Pt-Sn by adding a third metal (i.e., La, Ce, and Y) as a third promoter to modify the electronic and acidic properties of the supporter and the other added metals [22-28].

The production of a high-octane fuel by the isomerization process requires highly active, selective, stable, and harmless catalysts containing the expensive Pt metal. This work is related to the application of the concept of bimetallic catalysts in the preparation of a Zr-loaded Pt/HY-zeolite catalyst. Accordingly, the catalysts loaded with different ratios of metals were prepared for the purpose of studying their physical properties and performance during hydroisomerization reactions, and the cheap Zr metal was exploited as a partial substitute for the expensive Pt metal; the role of this less expensive metal in increasing the activity and selectivity as a result of the good dispersion of metals and the appropriate compatibility between acidic and metallic sites, and the stability of reduction. This allows catalyst producers to reduce the Pt content and reduce the cost of the catalyst. In addition, kinetic modeling was employed to represent the experimentally obtained data of the n-heptane hydroisomerization on the metal-loading catalyst. The newly developed kinetic model contains 16 component lumps and 43 reactions. Each of these components underwent several reactions according to proposed kinetic model.

2. Material and Methods

2.1 Materials

The following chemical reagents were purchased from commercial providers as follows: sodium aluminate (NaAlO₂: 50.9 wt% Al₂O₃+ 31.2 wt% Na₂O + 17.9 wt% H₂O) was provided by Sigma-Aldrich (Germany). Ludox AS-40 colloidal silica 40 wt% suspension in H₂O was provided by Sigma-Aldrich (USA). Sodium hydroxide pellets (NaOH): 99% was provided by CHEM-LAB (Belgium). Deionized water was provided by an Iraqi manufacturer. Ammonium chloride (NH₄Cl) was provided by SDFCL-SD FINE-CHEM (India). Hexachloroplatinic acid H₂PtCl₆ was provided by Sigma-Aldrich (USA). Zirconyl nitrate, ZrO(NO₃)₂.H₂O, 99.5% was provided by Oxford Lab Chem (India). Hydrogen (99.9%) was provided by Petroleum R&D Center (Baghdad, Iraq). N-heptane 99% was provided by CHEM-LAB (Belgium).

2.2 Characterization techniques

X-ray diffraction (XRD) tests were conducted by the SHIMADZU Laboratory XRD-6000 diffractometer (Japan), with a scan rate of 0.2 degrees, Cu (15406 Å), voltage 40 KV, and current 30 mA. The morphology of the framework structure of different catalysts and elemental compositions was observed by scanning electron microscope (SEM) associated with energy-dispersive X-ray spectroscopy (EDAX) using an FEI-Inspect S50 (University of Technology-Iraq). The specific surface areas of the synthesized catalysts were determined based on the Brunauer-Emmett-Teller (BET) method using a Q Surf 1600 analyzer (USA). A Shimzadu-1800 ART (Japan) Fourier-transform infrared (FT-IR) instrument was used to analyze the chemical bonds and the functional groups that were grafted onto the zeolite and loaded metals.

2.3 Catalyst synthesis

The synthesis of NaY-zeolite was achieved by a hydrothermal process utilizing laboratory-grade chemicals [29]. Then, the modification was first applied for removing the sodium ion from zeolite-NaY, which was performed by an ion-exchange process with an ammonium chloride salt solution to form NH₄-Y zeolite. To make the NaY-zeolite sites in an active acid form, the sodium ions or other cations must be replaced by protons (H⁺). The preparation of an active acidic zeolite first involves the conversion of Na-Y zeolite to NH₄-Y zeolite. The solid acid zeolite H-Y cannot be directly prepared from an aqueous solution as it is unstable under the acidic conditions needed [30]. Thus, this process was accomplished by an ion-exchange reaction mechanism; first, Na-Y zeolite was treated with an ammonium chloride salt solution with 0.5 mol of NH₄Cl to exchange the resided cations in the zeolite. This reaction was accomplished by heating the mixture at ~85°C for 2 h under continuous stirring and reflux conditions. The process of ion-exchange was reiterated for three consecutive times to remove most of the sodium ions; even then, the ion-exchange rarely exceeded 96%. The remaining 4% of the Na⁺ ions resided in the super-cage within the faujasite structure [31]. The following steps were performed: washing, drying, and calcining the ammonium form of zeolite at 450°C, leading it to decompose and release ammonia gas and leaving protons bonded to the oxygen atoms, creating a solid acid as a result of the existence of the proton (H⁺) [32]. To prepare the bifunctional bimetallic catalyst, the ammonium form of Y-zeolite was loaded with two metals (i.e., Zr and Pt) by the incipient wet impregnation method. The metal-modified rare earth catalysts showed significantly higher selectivity for isomerized products than unloaded catalysts. Generally, impregnation techniques have been used to prepare a variety of supported metal catalysts. Due to their active (de)hydrogenation functions and superior catalytic features, noble metals such as Pt rank as the most widely applied metallic components for bifunctional catalysts in the industrial applications of n-paraffin hydroisomerization [9,23,33,34]. The incipient wet impregnation method was performed by mixing the support (the ammonium form of zeolite) with a salt that contained metal ions at ~85°C and mixing for 3 h to make the metals ions migrate and relate to the zeolite structure to produce catalysts loaded with metallic ions. In our work, two metallic salts were used to prepare different mono- and bimetallic catalysts, as shown in **Table 1**. Hexachloroplatinic acid (H₂PtCl₆) was used as a source of Pt and zirconyl nitrate (ZrO(NO₃)₂.H₂O) as a source of Zr. The resulting material from the metal loading process was purified, using appropriate washing and drying steps under gas flow. The reduction temperatures are generally required to be greater than 300°C [35-37]. The reduction process was carried out in situ at an atmospheric pressure under a hydrogen flow rate of 5 L.h⁻¹. In addition, zirconium metal also shows excellent catalytic properties when it is loaded on an aluminosilicate support like zeolite, which makes the catalyst possess a good Lewis-type acidity that causes an increase in the production of isomers from paraffins in the hydroisomerization process [34-38]. Various characterization methods (i.e., XRD, SEM, EDX, FTIR, and BET) were used to analyze the characteristics of the synthesized catalysts. Testing the catalysts in a hydroisomerization unit was done by using standard n-heptane with an octane number of zero as a feed. Many experiments were conducted to test the catalytic activity and selectivity of the catalysts in a hydroisomerization rig. Gas chromatography-flame ionization detector (GC-FID) analysis was used to specify the isomerized products and their quantities.

Table 1. Composition and surface area of the prepared catalysts.

No.	Code	Catalyst Composition	Measured Surface Area (m ² /g)
1	Cat-1	Y-zeolite	481.9
2	Cat-2	Y-zeolite + 0.25 wt %Pt	
3	Cat-3	Y-zeolite + 0.50wt %Pt	312.6
4	Cat-4	Y-zeolite + 1.0wt %Pt	
5	Cat-5	Y-zeolite + 0.25 wt %Zr	
6	Cat-6	Y-zeolite + 0.50 wt %Zr	381.3
7	Cat-7	Y-zeolite + 1.0 wt %Zr	
8	Cat-8	Y-zeolite + 0.25 wt %Pt + 0.50 wt %Zr	
9	Cat-9	Y-zeolite + 0.50 wt% Pt + 0.50 wt %Zr	291.9
10	Cat-10	Y-zeolite + 0.25 wt %Pt + 1.0wt %Zr	

2.4 Catalytic experiments

The catalytic conversion of n-heptane was carried out over different HY-zeolite catalysts loaded with metals, as listed in **Table 1**. Operating the hydroisomerization rig began with inserting approximately 4 g of the catalyst particles of sizes 125-425 μm inside the stainless steel fixed-bed reactor (12-mm inner diameter and 30 cm in length), at the middle zone (i.e., stable temperature zone), between two layers of glass beads of 2-mm diameter, which were used to fill the dead volume of the reactor. For the purpose of identifying more information, it is possible to follow the attached supporting information file. The purpose of the glass beads was to make reactants at a balanced temperature in the stable heating zone of the reactor by warming up the reactants before their contact with the catalyst particles. Prior to the reaction, the catalyst reduction process was performed in situ at atmospheric pressure under a hydrogen flow rate of 5 L.h⁻¹ and at 350°C. The reactor was then pressurized with 1 MPa of hydrogen and cooled gradually to reach the specified reaction temperature of 250°C, and the hydrogen flow rate was set at the necessary value of the molar flow ratio H₂/C₇, which is equal to 5. As soon as the system stabilized at the desired conditions, the pump of the n-heptane feed was run at a desired C₇H₁₆ flow rate of 11.6 ml.h⁻¹. Afterwards, the reaction products were condensed, gathered at a time on a stream equal to 15 min and sent for GC analysis equipped with a flame ionization detector (FID) to detect the composition. Conversion, selectivity, and yield were calculated using the following equations:

$$\text{Conversion} = \frac{\text{Initial moles of } n\text{-heptane} - \text{Final moles of } n\text{-heptane}}{\text{Initial moles of } n\text{-heptane}} \quad (1)$$

$$\text{Selectivity} = \frac{(\text{Total moles of isomers})}{\text{Initial moles of } n\text{-heptane} - \text{Final moles of } n\text{-heptane}} \quad (2)$$

$$\text{Yield} = \frac{\text{Total moles of isomers}}{\text{Initial moles of } n\text{-heptane}} \quad (3)$$

3. Results and Discussion

3.1 Characterization of the solid catalysts

3.1.1 X-Ray diffraction (XRD) analysis

The XRD analysis of the synthesized zeolite sample exhibited a successful crystalline structure, as shown in **Fig. 1**, indicating that the structure had approximately the same pattern and equal major peaks in comparison with the XRD pattern of the standard zeolite faujasite Y-type referenced by

the International Zeolite Association (IZA) [29, 39]. The major peaks of the XRD pattern of the synthesized sample were in identical positions with the major peaks of the standard faujasite, which confirmed that the synthesized sample was successfully prepared and had a faujasite framework structure [29, 39].

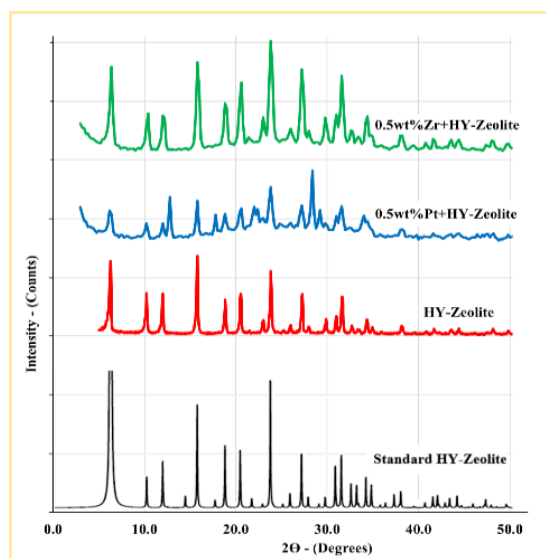


Fig. 1. XRD-pattern of the synthesized and metal-loaded zeolite-Y catalysts.

In addition, modification with a small amount of Pt and/or Zr metals could neither affect the overall structure of the zeolite-Y nor introduce structural changes in the solid lattice because the major X-ray diffraction of the peaks in the XRD patterns remained at the same positions (i.e., 2θ), and no additional peaks were detected in the XRD patterns of Pt/HY and/or Zn/HY, indicating that the samples were pure Y-zeolite form. A change was observed only in the relative intensity of the multiple diffraction peaks, which was due to the fact that metals can act as impurities and can cause X-ray deflection and lower peak intensities, which is attributed to the transition metals loaded into the zeolite frameworks resulting in a decrease in zeolite crystallization. Moreover, a partial collapse of the Y-lattice could also be expected and caused a decrease in solid crystallinity and an increase in the amorphous materials; thus, the flat baseline that appeared in the XRD patterns of Pt/HY or Zn/HY was higher compared to that of the traditional HY-zeolite. This was due to calcining the ammonium form of Y-zeolite and then reducing the metals at high temperatures during the preparation processes.

3.1.2 BET-surface area analysis

Brunauer–Emmett–Teller (BET) surface area measurements for solids are dependent on the gas isothermal phenomenon (i.e., adsorption and desorption). These two processes are based on the same rule, but one is the reverse of the other. Adsorption occurs when gas molecules contact the surface of a solid and a layer of adsorption material is formed, such as the accumulation of nitrogen gas molecules on the surface of Y-zeolite. A zeolite sample (0.2 g) in powder form was loaded into a bulb-shaped quartz tube. The sample tube was then heated to about 350°C to drive out the gas by means of a furnace. A vacuum outgassing step was performed prior to the BET measurement for 480 min to remove contaminants. Then the corrected weight of the zeolite sample was taken after the drying step. For continuous

outgassing conditions, the accuracy of the BET surface area analysis is $\pm 10\%$. During the test, the N_2 molecules were adsorbed onto the sample surface, and this adsorption gas liquefies on the solid at the adsorption temperature (-196°C), followed by a pressure drop in the BET system. By repeating this process, the data measuring pressure change with the amount of adsorbed gas can be collected. In fact, increasing the amount of metal loaded onto the surface of the catalyst prevents nitrogen molecules from entering the catalyst structure, and it is logical that this would reduce the area calculated using this method. The specific surface area of the utilized HY-zeolite samples was found to be $481.9\text{ m}^2/\text{g}$. A group of manufactured catalysts was examined to verify the effect of metal loading on the textural properties of the solid catalyst and the obtained data are listed in **Table 1**. Results of BET tests showed that the BET-surface area of the HY-zeolite sample, which possesses a high surface area and is in agreement with the standard values of HY-zeolite [29,38]. In addition, the surface area of the HY-zeolites loaded with metals showed a decrease in the surface area, taking into account that the zirconium-loaded catalyst had a higher surface area than the platinum-loaded catalyst. The reason for this is that the metal atoms may have closed some of the zeolite pores, and this is identical to what has been documented [40]. In addition, the bimetallic catalyst (Cat-9) had a surface area of $291.9\text{ m}^2/\text{g}$, as it was loaded with two types of metals.

3.1.3 Energy dispersive X-ray (EDX) analysis

The indicative bulk Si/Al ratio within the lattice of synthetic zeolite-Y was calculated according to the results of EDX and reached 2.2, which is in a good agreement with Matti et al. [41] and Souza et al. [42]. The synthesized NaY-zeolite passed through three stages of ion-exchange treatments using an ammonium chloride salt solution to remove the sodium ion and convert it to ammonium form of Y-zeolite. EDX analysis was performed after this treatment to measure the sodium concentration within the zeolite framework structure, and the test showed that the concentration dropped from 8.5 wt% to about 0.45 wt%, which confirmed the success of the treatment. Then, the ammonium form of Y-zeolite was loaded with metals to prepare monometallic and bimetallic catalysts according to the metal-loading calculations and using the wet incipient impregnation method. The concentration of the loaded metals was measured by EDX analysis. Several samples were prepared and examined, as presented in **Table 1**. The EDX tests showed a deviation of the measured concentrations from the mathematically calculated concentrations of no more than 5-10%, which is considered acceptable. **Fig. 2** shows different samples of the prepared catalysts loaded with one metal and/or two metals tested using EDX analysis. The EDX spectrum demonstrates the peaks corresponding to the energy levels, and each of these peaks is unique to a single element; the higher the peak in the spectrum, the higher the concentration of the element in the sample. It is therefore possible that EDX analysis can give indicative elemental analysis such as of Al, Si, O, Na, Pt, or Zn on specific regions located on the outer surface of the crystal.

3.1.4 Scanning electron microscopy (SEM) analysis

The morphology of the framework structure of the synthesized Na-Y zeolite (Cat-1), Y-zeolite loaded with 0.5 wt% Pt (Cat-4), Y-zeolite loaded with 0.5 wt% Zr (Cat-7), and the bimetallic catalyst Cat-9 (Y + 0.5 wt% Pt + 0.5 wt% Zr) were investigated with scanning electron microscopy, and the SEM images are shown in **Fig. 3**. It can be seen that clusters of

zeolite particles consist of semi-cuboidal and spherical crystals of 2-5 μm in length, separated and not agglomerated. These results are consistent with the results of the X-ray diffraction analysis. In fact, zeolite crystallites seem more clearly with high homogeneity. In general, no obvious changes

were detected in the morphology of the bimetallic catalyst Cat-9, demonstrating that no crystalline transformation had taken place throughout the dispersion of the metals within the Y-structure, which agrees with the results of Nsaif et al. [43].

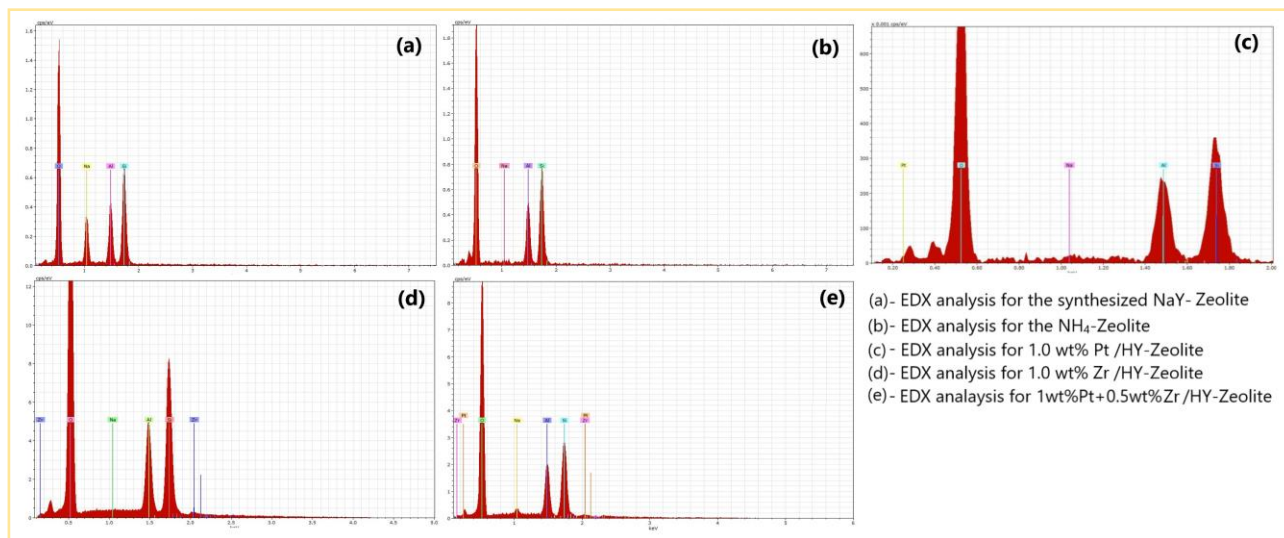


Fig. 2. Typical EDX spectra of the synthesized and metal-loaded zeolite-Y samples.

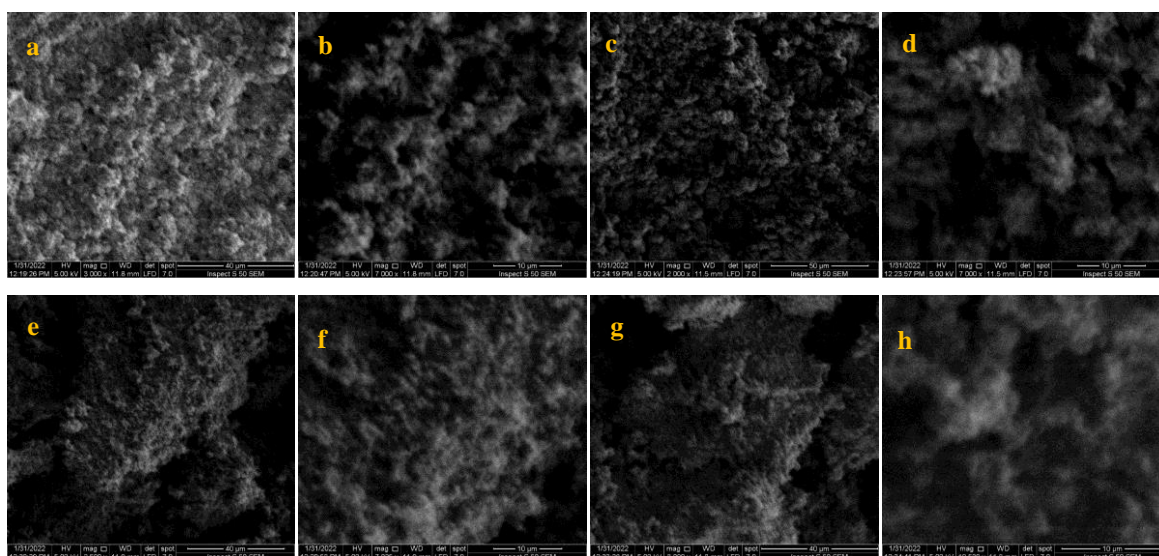


Fig. 3. SEM-images with 40 and 10 μm magnification for (a) and (b) the synthesized HY-zeolite, (c) and (d) 0.5 wt% Zr/HY-zeolite, (e) and (f) 0.5 wt% Pt/HY-zeolite, (g) and (h) (0.5 wt% Pt + 0.5 wt% Zr)/HY-zeolite.

3.1.5 Fourier-Transformed infrared spectroscopy (FT-IR) analysis

FT-IR characterization was used to analyze the chemical bonds and functional groups that are available in the zeolite lattice. In fact, the same set of manufactured catalysts mentioned in **Table 2** were examined using FT-IR analysis with an aim of investigating the loaded metals sites within the zeolite framework structure. The results are presented in **Fig. 4a and b**. The FT-IR spectrum for NH_4Y -zeolite (Cat-1) had wavenumbers ranging from 600-4000 cm^{-1} , as shown in **Fig. 4a**, in which the H-O-H bending vibration of bound water appeared at a wavenumber of 1631 cm^{-1} , indicating the presence of adsorbed water in the zeolites [44]. The peak wavenumber 983.7 cm^{-1} can be assigned to the antisymmetric stretching vibration of Si-O. The absorption bands at 770, 678, 574, and 480 cm^{-1} can be ascribed to an O-Si-O stretching

vibration, Si-O symmetrical stretching vibration, O-Al-O stretching vibration, and Si-O-Si bending vibration, respectively, as well as the 1427 cm^{-1} band assigned to the bending vibration of NH_4^+ [40, 44-46].

In addition, the FT-IR spectrum of NH_4Y -Zeolite loaded with 0.5 wt% Pt (Cat-4), as shown in **Fig. 4b**, with a wavenumber range of 400-600 cm^{-1} , has absorption bands at wavenumbers 520 and 578 cm^{-1} , which can be attributed to the impact of the platinum groups (Pt-O-Si), confirming that the Pt atoms were successfully incorporated into the zeolite frameworks; this is in agreement with the results observed by other authors [47, 48]. On the other hand, the FT-IR spectrum of NH_4Y -Zeolite loaded with 0.5 wt% Zr (Cat-7) has the absorption band at wavenumber 420.48 cm^{-1} , which can be ascribed to the Zr ion vibrations of the (Zr-O-Si) bonds, which suggests that the Zr atoms have been successfully

incorporated into the zeolite framework, consistent with the results observed by [40, 45, 49]. Furthermore, the FT-IR spectra of the bimetallic catalyst (Cat-9) exhibited two clear peaks at wavenumbers 424.3 and 474.4 cm^{-1} . The absorption band at wavenumber 424.3 cm^{-1} can be ascribed to the Zr ion for vibrations of the Zr–O bonds that had shifted from

wavenumber 420 to 424 cm^{-1} (in a single metal loading), in agreement with the results observed by [26,49]. The absorption band at wavenumber 474.4 cm^{-1} can be ascribed to the Pt ion, which shifted from wavenumber 478 (in a single metal loading), which is consistent with other results [47, 49].

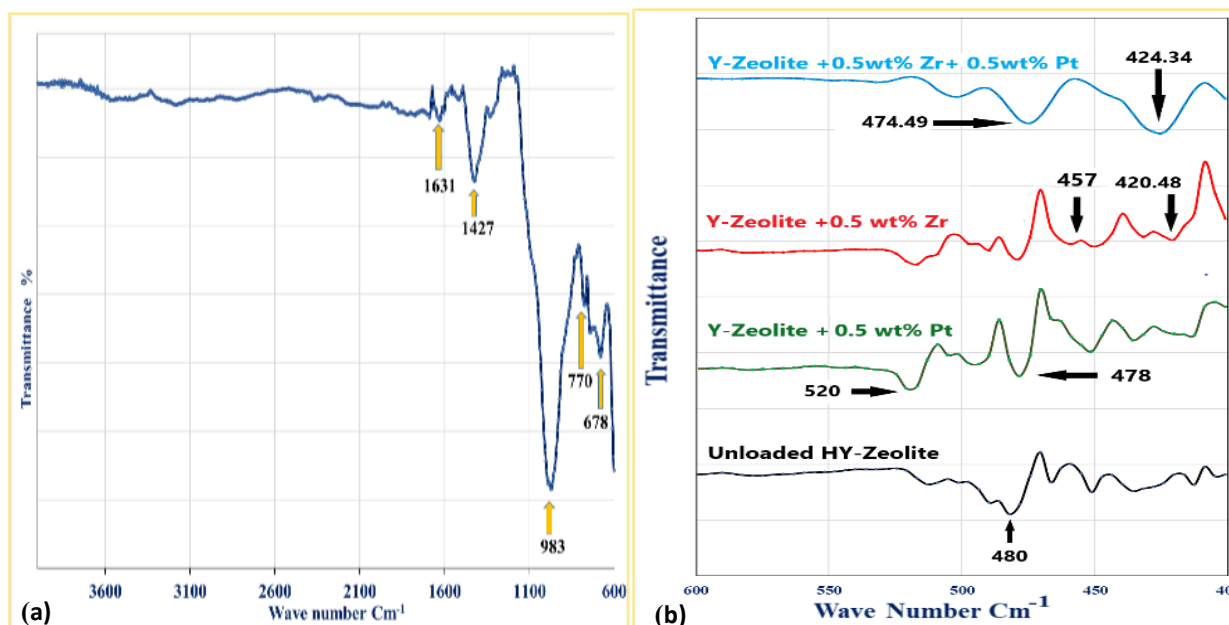


Fig. 4. (a) FT-IR spectrum of NH_4Y -zeolite, (b) FT-IR spectra of the synthesized and metal-loaded zeolite-Y catalysts.

3.2 The performance of catalysts in n-heptane hydroisomerization reactions

To study the effect of Pt and Zr metals loaded inside zeolite crystals on the n-heptane hydroisomerization as a model reaction, a number of experiments were conducted using Y-zeolite catalysts loaded with different proportions of metals, as given in Table 1. Consequently, 10 experiments

were carried out at a temperature of 250°C and 1 MPa. Their results are tabulated in Table 2, and two other experiments completed at temperatures of 225°C and 275°C using a bimetallic catalyst are tabulated in Table 3, which had the best behavior during the experiments compared with the rest of the manufactured catalysts for the purpose of calculating the kinetics and reactions model.

Table 2. Results of n-heptane hydroisomerization experiments at 1 MPa and 250°C (products in mol%)

Products	Cat-1	Cat-2	Cat-3	Cat-4	Cat-5	Cat-6	Cat-7	Cat-8	Cat-9	Cat10
C1-C3	16.11	12.47	8.34	9.23	16.35	15.34	14.40	13.00	9.12	16.00
iC4	3.47	4.04	4.61	6.12	3.95	7.33	9.43	5.11	6.31	8.23
nC4	8.45	5.46	3.41	2.03	8.62	4.45	8.66	3.29	2.34	3.34
C4=	1.43	1.06	0.46	0.10	1.26	1.06	0.84	0.28	0.13	0.16
iC5	1.92	2.00	2.67	1.23	2.45	2.64	1.56	2.81	2.39	1.55
nC5	3.80	3.01	2.91	0.71	4.11	3.01	0.76	1.07	0.86	2.12
C5=	0.72	0.39	0.25	0.13	0.43	0.24	0.17	0.36	0.29	0.44
iC6	1.41	0.73	0.53	0.25	0.84	0.61	0.25	0.55	0.60	0.53
nC6	1.68	1.09	1.62	0.22	1.34	0.72	0.15	0.19	0.15	0.58
C6=	0.32	0.23	0.11	0.00	0.31	0.18	0.12	0.23	0.19	0.22
iC7	44.57	53.10	58.00	61.41	45.90	47.50	28.56	57.23	60.90	40.49
nC7	15.31	15.81	16.89	18.57	13.55	17.99	34.88	15.60	16.50	26.07
C7=	0.81	0.61	0.20	0.00	0.89	0.43	0.22	0.28	0.22	0.27
Totals	100.00	100.00	100.00	100.00	100.00	100.00	100.00	100.00	100.00	100.00
Conversion	83.80	83.3	82.22	80.54	85.56	81.12	64.23	83.51	82.61	73.04
Selectivity	61.30	71.87	80.04	85.68	62.11	71.60	61.96	78.67	84.98	69.55
Yield	51.37	59.87	65.81	69.01	53.14	58.08	39.80	65.70	70.20	50.80
Total of isomers	51.37	59.87	65.81	69.01	53.14	58.08	39.8	65.7	70.2	50.8

3.2.1 Hydroisomerization experiments using monometallic Pt/HY-zeolite catalysts

The hydroisomerization of n-heptane was performed using an unloaded HY-zeolite (Cat-1) catalyst, together with three further experiments for Pt/HY-zeolite catalysts (i.e., Cat-2, Cat-3, and Cat-4) loaded with 0.25, 0.5, and 1 wt% Pt,

respectively, as displayed in Table 2. These data are plotted in Figs. 5a and 6a. It is clear that fresh HY-zeolite (Cat-1) showed good isomerization activity with 83.8 mol% for conversion and a modest selectivity to isomers at 61.3 mol%. In fact, the HY catalyst has a high catalytic activity but a moderate ability for yielding isomers. It also had a high cracking ability due to the

very high acidity of the Brønsted type, giving a logical reason to the high conversion with high low molecular weight products of (C₁-C₃), which were 16.11 mol% of the products compared to other loaded zeolites catalysts. The availability of enough metal sites is critical to maintaining the dehydrogenation-hydrogenation function, which is significant for achieving high isomerization rates [50]. In addition, it can be seen in Fig. 5a that the selectivity and yield of the hydroisomerization reaction were dramatically enhanced with the increase of the content of the Pt metal within the zeolite catalysts. The effect of the Pt metal on the reaction conversion caused a slight decrease from 83.8% using the unloaded catalyst (zero Pt content) to 80.54 mol% using 1 wt% of Pt. It can be concluded that Pt-loaded metal increases the activity of the catalyst, but at the same time reduces the

overall acidity of the Brønsted acid sites in the zeolite, which causes a decrease in the cracking capability and an increase in the isomerization trend. This slight reduction in conversion may also be due to the decrease in the zeolite surface area, whereby the Pt ions can somewhat close several of the pores and cavities available in the zeolite structure. BET analysis showed that the Pt-loaded zeolite possesses a lower surface area than that of nonmetal-loaded zeolites. Moreover, at the range from 0.25 to 0.5 wt% of the Pt loaded metal, the selectivity increased remarkably and led to a strong enhancement in the production of isomers, which increased from 71.87% at Cat-2 to 80.04% at Cat-3, and 85.68 mol% at 1% Pt in Cat-4, confirming that the selectivity mainly depends on the Pt metal content, which had been proven by [6, 51].

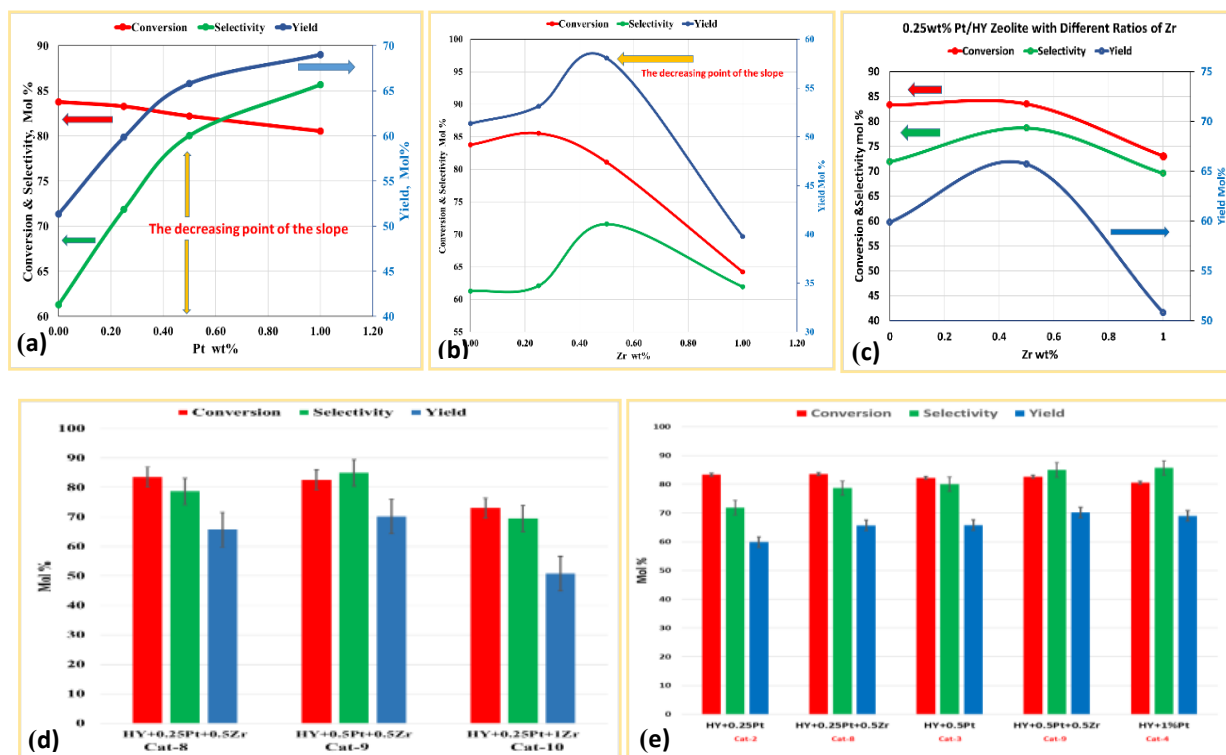


Fig. 5. Catalytic performance at 250°C and 1 MPa using different loading ratios of metals on HY-zeolite: (a) Pt metal, (b) Zr metal, (c) bimetallic catalyst with constant ratio of Pt (i.e., different loading ratios of Zr), (d) bimetallic Pt-Zr/HY catalysts, (e) a comparison between the monometallic Pt/HY catalysts and the bimetallic Pt-Zr/HY catalysts. Note: Error bars in Figs. 5d and e have been added for adequate comparison.

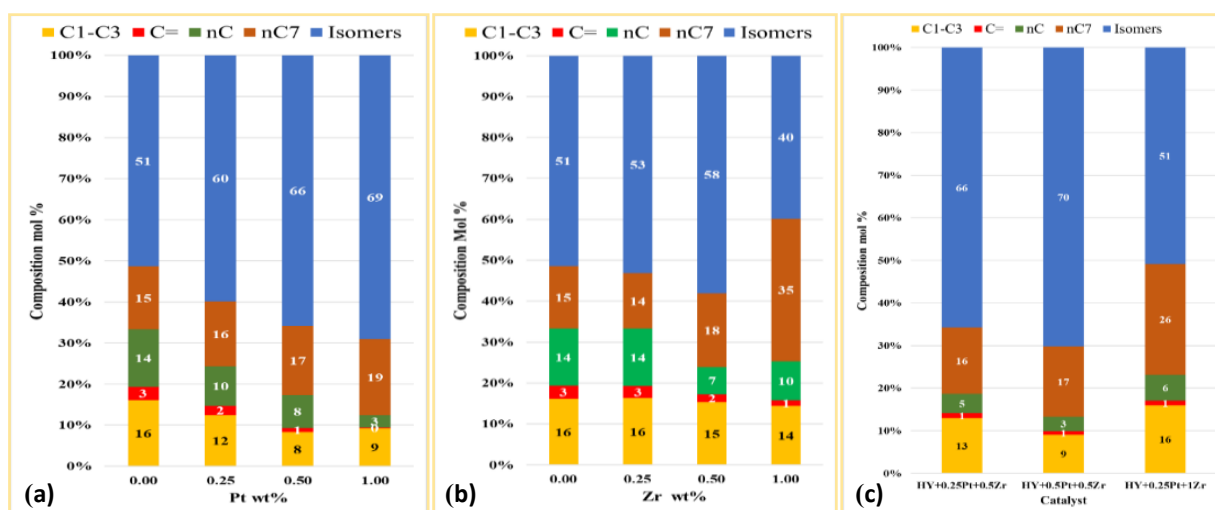


Fig. 6. Product compositions of n-heptane isomerization processes at 250°C and 1 MPa using the catalysts: (a) Pt/HY-zeolite, (b) Zr/HY-zeolite, and (c) bimetallic Pt-Zr/HY.

On the other hand, in the loading range from 0.5 to 1 wt% Pt, the slope of the curve was less than that in the first interval (i.e., 0-0.5) wt% Pt, meaning that the yield improved only slightly, which confirms that it is not economical to use Pt above 0.5 wt% as a result of its low impact and high cost. Pt metal contributes to reducing the acidity of zeolite and dropping the surface area. These results were in a good agreement with other studies [6,52]. Furthermore, the results of the experiments agreed with Sinfelt and the conclusions of other authors, who had reported that even at the lowest platinum content, the dehydrogenation activity of the catalyst was sufficient to maintain the equilibrium between paraffin and olefin on the catalyst surface [22-28]. The isomerization rate is therefore controlled by the acidic activity of the catalyst [53]. Loading zeolite with a large concentration of Pt is not recommended because it causes hydrogenolysis of hydrocarbons, which leads to an increase in the low molecular weight gas products and also decreases the production yield of isomers [6,54,55]. Additionally, Pt inhibits coke formation by improving Lewis acid sites and providing a dehydrogenation/hydrogenation function. The results of the experiments are consistent with the literature that explains what happens when Pt is loaded at high levels [34,56]. According to the bifunctional mechanism, dehydrogenating the hydrocarbons can make the hydrogen react with isomerized olefins, leading to an increase in isomer yield. In addition, it cleans the catalyst surface of heavy cracked hydrocarbons by saturating them with hydrogen, which reduces coke formation, making the role of Pt essential in the lifespan of catalysts [52, 57]. It can also be observed in **Fig. 6a** that olefins decreased with an increase in the amount of Pt loaded within the catalyst, as a result of the active role of Pt in saturating the olefins. The normal cracking products decreased with an increase of Pt because some of them were converted into isomers by the effect of Pt. All these findings were in agreement with the conclusions of many other researchers [58, 59].

3.2.2 Hydroisomerization experiments using monometallic Zr/HY-zeolite catalysts

The results of three experiments for the three HY-zeolite-based catalysts (i.e., Cat-5, Cat-6, and Cat-7) loaded with 0.25, 0.5, and 1 wt% Zr metal are included in **Table 2**. These data are plotted in **Figs. 5b** and **6b** and are compared with that of unloaded HY-zeolite (Cat-1). It is clear from these figures that the Zr metal had a positive effect on both the selectivity and yield of the hydroisomerization reaction. The reaction conversion slightly increased from 83.8% HY-zeolite with zero percentage Zr (Cat-1) to 85.56 mol% for 0.25 wt% Zr/HY-zeolite (Cat-5). The reason for the increased conversion stems from the fact that a small amount of Zr leads to an increase in acidity (i.e., Lewis type), which increases the catalyst activity and increases the conversion. Therefore, the addition of Zr metal enhanced the yield of the isomers from 51.37% in Cat-1 to 53.14 mol% in Cat-5. In the loading range from 0.25 to 0.5 wt% Zr, the selectivity clearly increased from 62.1% at 0.25 wt% Zr to 71.6 mol% at a 0.5 wt% Zr loading ratio, indicating the effect of Lewis acid sites generated by the Zr metal that led to the increased production of isomers. However in the same range, conversion tended to decrease slightly from 85.56% in Cat-5 to 81.12 mol% in Cat-6. This decrease was due to the drop in the acidity of the zeolite (Brønsted type), which began to decrease as the Zr metal occupied its positions and some of pores were closed, which led to a decrease in the surface area, as previously proven in the BET analysis. However the selectivity seems to have increased, causing an increase in the yield of the resulting isomer from 53.14% to

58.08 mol% as the Zr content increased from 0.25 to 0.5 wt%, leading in a noteworthy improvement in the performance of the catalyst.

In the range of 0.5 to 1 wt% Zr, it is clear from **Fig. 5b** that the conversion significantly decreased from 81.12% to 64.23 mol% as a result of the acidity deterioration of zeolite catalyst. Moreover, the conversion decreased because the increase in the Zr-loaded atoms led to blockage of some pores on the surface of the zeolite, and the Zr cations lowered the acidity of the Brønsted, which is responsible for the acidity of the HY-zeolite catalyst. Therefore, these results confirmed that it is not appropriate to use Zr metal above 0.5 wt% in loadings over zeolite catalysts. However, Zr increases Lewis acid sites and contributes to higher yields of isomers, especially in the range from 0.25-0.5 wt% Zr, and Kitaeva et al. reached the same findings when they used ultra-stable Y-zeolite [26]. Finally, the spectrum of products of n-heptane hydroisomerization over Zr-loaded HY zeolite, as presented in **Fig. 6b**, shows that the number of isomers increased with increasing percentages of Zr metal until it reaches 0.5% by weight. At the same time, the cracking of products such as gases (C₁-C₃) gradually decreased. In addition, olefins and normal hydrocarbons decreased with an increase of Zr. This occurred as a result of the active role of Zr, which enhanced the Lewis acidity and reduced the high Brønsted acidity of the HY-zeolite, which is responsible for cracking.

3.2.3 Hydroisomerization experiments using bimetallic Pt-Zr/HY-zeolite catalysts

In the three experiments using bimetallic catalysts (i.e., Cat-8, Cat-9, and Cat-10), metal loading ratios were carefully designed to determine the effect of changing one metal while keeping the concentration of the other metal constant. Results of the three experiments are listed in **Table 2**. The obtained data from the experiments are plotted in **Figs. 5d** and **6c**. These graphs clearly demonstrate the effect of loading different ratios of Pt and Zr metals on the activity and selectivity of the hydroisomerization reaction. From the results obtained, the difference was obvious in the behavior of the Cat-8 and Cat-9 catalysts during the reaction, which have the same Zr content of 0.5 wt%, due to the effect of changing the concentration of the Pt metal from 0.25 to 0.5 wt%. The reaction conversion slightly decreased from 83.51% in Cat-8 to 82.61 mol% in Cat-9, but the selectivity clearly increased with an increase of Pt from 78.67% in Cat-8 to 84.98 mol% in Cat-9. This resulted in a strong enhancement in the yield from 65.7 to 70.2 mol% as a result of the Pt atoms providing the dehydrogenation-hydrogenation function that improved the conversion of long hydrocarbon chains into isomers. However, some of the Brønsted sites were occupied by Pt cations, which caused a decrease in the Brønsted acidity of the zeolite and may reduce the overall reaction conversion. Comparison of Cat-9 and Cat-10 showed the effect of simultaneously changing the concentration of the two metals on the performance of the HY-catalyst during the reaction. Decreasing the Pt content from 0.5 to 0.25 wt% and increasing the Zr content from 0.5 to 1.0 wt% significantly deteriorated the overall conversion of the reaction from 82.61% in Cat-9 to 73.04 mol% in Cat-10. The selectivity also decreased from 84.98% to 69.55% respectively, due to the high content of Zr that crossed the threshold and caused negative structural and electronic changes to the zeolite, as it closed a large portion of pores and decreased the strong Brønsted acidity of the zeolite considerably, leading to a large fall in the yield of isomers from 70.2% to 50.8 mol%, respectively. These results confirm that the optimum concentration of Zr should be less

than 1.0 wt% and in the range from 0.25-0.5 wt%. The comparison between Cat-8 and Cat-10 showed the effect of changing the Zr concentration but keeping the Pt content constant; the conversion and yield deteriorated with an increase of Zr. This comparison is discussed in depth later.

Fig. 6c demonstrates a comparison of n-heptane hydroisomerization products by using three bimetallic catalysts, showing the increase of the isomers produced when increasing the Pt content from 0.25 in Cat-8 to 0.5 wt% in Cat-9 at a constant Zr content of 0.5 wt%. At the same time, the broken products, such as C₁-C₃ gases and normal cracking products (nC), decreased with increasing amounts of Pt, as a result of the active role of Pt in increasing the number of isomers. Increasing the Zr metal content from 0.5 wt% in Cat-8 to 1% in Cat-10 with the two catalysts containing the same amount of Pt (0.25 wt%), the isomers decreased significantly, with a significant increase in C₁-C₃ gases due to the effect of the high content of Zr metal. This blocked some pores of the catalyst and the effect of cracking, which was created via the increased acidity of the Lewis type generated by the high content of Zr metal. **Fig. 6c** also shows that the Cat-9 yielded the best spectrum distribution for the products of the heptane hydroisomerization process. Thus, it can be selected as the best bimetallic catalyst, achieving the highest yield of isomers at 70.2, along with 82.61% and 84.98 mol% for conversion and selectivity, respectively.

3.2.4 Impact of Zr metal in enhancing the selectivity and yield of bimetallic catalysts in the hydroisomerization process

As mentioned earlier, Zr metal increases the number of Lewis acid sites. The effect of Zr metal appeared clearly in the results of the experiments (see **Table 2**) that compare three catalysts with a fixed content of Pt metal and a gradual increase in the content of Zr (i.e., 0., 0.50, 1.0 wt%). In Cat-8 (containing 0.5% Zr), the Zr contributed to an increase in the selectivity and yield of isomers compared to Cat-2 without Zr, whereby the yield increased from 59.87 to 65.7 mol%, confirming the effect of Zr on enhancing the catalytic activity. The data are plotted in **Fig. 5c**, which illustrates that the catalyst Cat-2 (composed of 0.25 wt% Pt/HY) exhibited 83.3, 71.87, and 59.87 mol% of the catalytic parameters of conversion, selectivity, and yield, respectively. These catalytic parameters improved greatly when the catalyst (Cat-2) was loaded with 0.5 wt% Zr (in Cat-8), causing these three aforementioned parameters to improve to 83.51, 78.67, and 65.70 mol%, respectively. This demonstrates the impact of Zr in enhancing the yield of isomers, which was caused by the new Lewis acidity generated by the electronic features of the added Zr metal. This also occupied some for zeolite Brønsted acid sites, leading to a slight decrease in the strong Brønsted acidity that causes cracking. Further evidence of the effect of the Zr metal occurred when a comparison was made between equal Pt content Cat-3 and Cat-9 catalysts containing 0.5 wt% Pt. The Zr content increased from 0% in Cat-3 to 0.5 wt% in Cat-9. The catalytic parameters of Cat-3 were 82.22, 80.04 and 65.81 mol% for conversion, selectivity and yield, respectively, while the catalytic parameters of Cat-9 were 82.61, 84.98 and 70.20 mol%, respectively. Thus, the conversion improved slightly as a result of the increased acidity of the Lewis type, but the selectivity increased significantly, leading to an enhancement in the yield from 65.8% to 70.2 mol%. **Fig. 5e** shows a comparison of the catalytic performance of the

bimetallic catalysts with the monometallic Pt/HY catalysts. The striking result is that the catalytic features of the bimetallic catalysts performed almost equally with the high-content Pt catalyst. Cat-8 (0.25 wt% Pt) compared to Cat-3 (0.50%Pt) had approximately equal activity, and Cat-9 (0.5 wt% Pt) compared to Cat-4 (1 wt% Pt) also has approximately the same activity. These findings underscore the importance of employing the cheap and available Zr metal in making zeolite-based catalysts more active, productive, and stable during reactions. At the same time, the Zr metal played a key role in reducing the content of the expensive and rare Pt metal in the formation of bimetallic catalysts, making the hydroisomerization process more economical. In addition, a small amount of Pt (as low as 0.25 wt% with 0.5 wt% Zr) can be used as an active and isomerization-selective catalyst, as in Cat-8, which had a performance approximately similar to the expensive Cat-3 catalyst (0.5 wt% Pt/HY), making the goal of reducing the Pt content both real and practical.

3.2.5 Hydroisomerization experiments using the optimally selected catalyst at three reaction temperatures

Three experiments were conducted to investigate the hydroisomerization of n-heptane to determine the optimum Cat-9 bimetallic catalyst at three temperatures. The results are given in **Table 3** and are also plotted in **Figs. 7a** and **b**.

Table 3. n-heptane hydroisomerization experiments using the catalyst Cat-9 at three temperatures (mol%)

Reaction Temperature	225°C	250°C	275°C
Conversion	71.15	82.61	89.26
Selectivity	86.07	84.98	60.14
Yield	61.24	70.20	53.68

It is clear that the conversion of n-heptane to the products increased with increasing reaction temperature, and the selectivity of the isomers decreased slightly from 86.07% at 225°C to 84.98 mol% at 250°C. However, the selectivity decreased sharply at 275°C, falling to 60.14 mol%, which makes the range 225-250°C more suitable for the hydroisomerization process because it provides high selectivity. The yield curve had a maximum point near 250°C, realizing the highest yield of 70.2 mol%, and the yield decreased both before and after this point, but it decreased significantly at temperatures higher than 250°C. The data of the three experiments were used in calculating the kinetics parameters and predicted values of the products. **Fig. 7b** illustrates the composition of the products of three hydroisomerization experiments of n-heptane at three temperatures (i.e., 225, 250, and 275°C). The catalyst showed a high cracking ability at 275°C, which yielded a higher percentage of low molecular weight compounds, especially C₁-C₃ gases. The cracking pathway increased with rising reaction temperatures, and the isomers increased with decreasing temperature. In addition, at the high temperature of 275°C, some olefins seemed to have been unsaturated completely despite the effect of the high temperature in increasing the cracking path. Also, it appears that the moderate pressure of hydrogen (1 MPa) was not sufficient to fully saturate the olefins, as the hydrocracking process must be performed under a high hydrogen pressure.

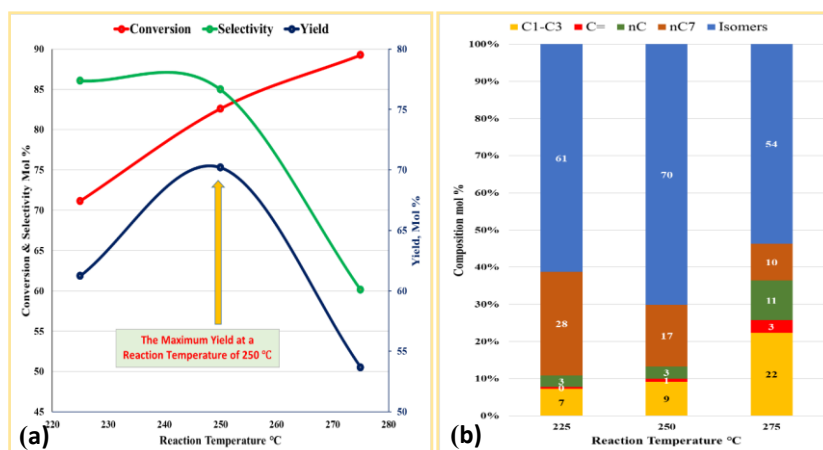


Fig. 7. (a) Effect of temperature on the catalytic performance of the Cat-9 catalyst, (b) composition of the products of hydroisomerization of n-heptane using the Cat-9 catalyst at different reaction temperatures under a pressure of 1 MPa.

3.3 Reaction mechanism and kinetics

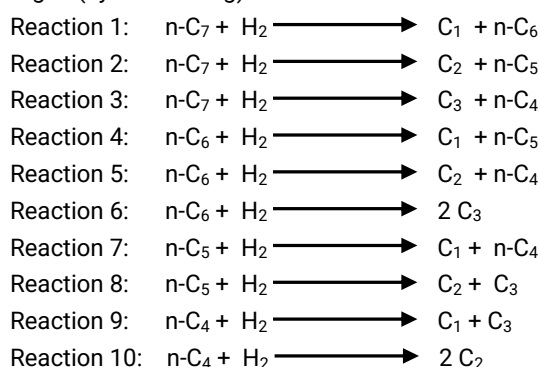
3.3.1 Proposed reaction kinetics of n-heptane isomerization

A kinetics model was proposed and identified to represent the experimental results obtained at various operating conditions, according to the literature [60].

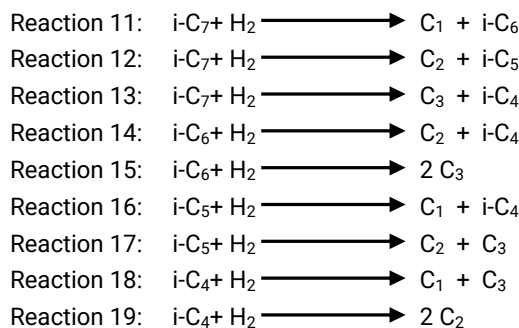
The 16 n-heptane hydroisomerization product components that were experimentally found in the products, with different concentrations, are listed as follows: H₂, C₁, C₂, C₃, iC₄, nC₄, C₄=, iC₅, nC₅, C₅=, iC₆, nC₆, C₆=, iC₇, nC₇, C₇=.

The probable reaction paths that give rise to these hydrocarbons are as follows:

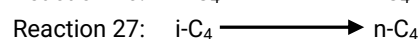
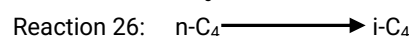
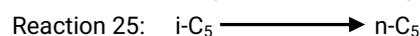
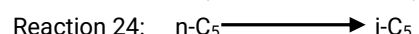
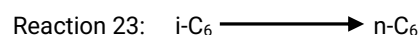
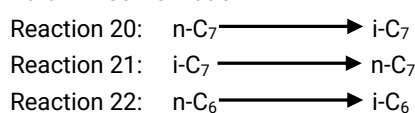
n-paraffin cracking: Cracking with the presence of hydrogen (hydrocracking).



i-paraffin cracking with hydrogen



Paraffin isomerization



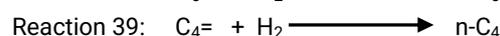
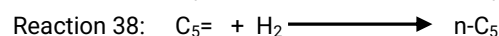
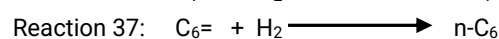
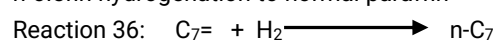
n-paraffin dehydrogenation



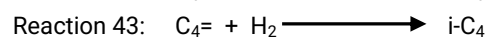
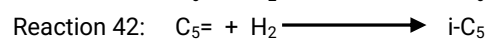
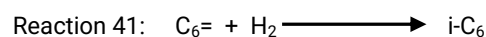
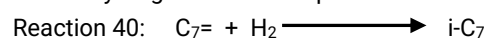
i-paraffin dehydrogenation



n-olefin hydrogenation to normal paraffin



i-olefin hydrogenation to iso-paraffins



3.3.2 Mathematical model

The following differential equation was employed to represent the differences in the molar flow rate for the reaction mixture within the reactor bed [60]:

$$\frac{dF_i}{dw} = - \sum_j^m S_{ij} r_j \quad (4)$$

where *i* refers to the component *i*, *j* represents the number of reactions, *F_i* is the molar flow rate of *i*th component (mol/h), *w*

is the catalyst weight (g), $r_j = K_i C_i$, r_j is the reaction rate per catalyst mass (mol/h. g_{cat}), C_i is the molar concentration of the i^{th} component (mol/m³), and S_{ij} is the stoichiometric coefficient for the i^{th} component participating in the j^{th} reaction. The Arrhenius equation was used to represent the variation in the reaction rate constants with temperature:

$$k_j = k_j^0 \exp\left(-\frac{E_{Aj}}{RT}\right) \quad (5)$$

where R is the gas constant 8.314 (J/mol^oK), T is the temperature (^oK), k_j^0 is the pre-exponential factor (m³/g_{cat}.h), and E_A is the activation energy (J/mol).

The model involved solving 16 ordinary differential equations, one equation for each component. A differential evaluation-optimization algorithm was used to estimate a global optimum set of kinetic parameters by minimizing the objective function (minimum mean relative error); the mean relative error (MRE) was calculated using Eq. 6 [61]:

$$MRE = \frac{1}{N \times M} \sum_{j=1}^M \sum_{i=1}^N \left(\frac{y_{ij}^{exp} - y_{ij}^{pred}}{y_{ij}^{exp}} \right) \quad (6)$$

Where N , M , y_{ij}^{exp} , and y_{ij}^{pred} are the components' number, dataset number, experimental mol fraction values, and predicted mol fraction values, respectively. All computations within this study were predicted using programs coded using MATLAB 2015a software. Genetic algorithm optimization was used to estimate the optimum set of kinetic parameters. MATLAB functions GA and ode45 were used in optimization and integration.

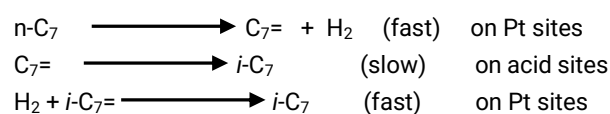
Stochastic optimization methods are optimization algorithms that incorporate probabilistic (i.e., random) elements to diversify and intensify the search space of the decision variables. Further, the injected randomness may provide the necessary impetus to move away from a local solution when searching for a global optimum. Stochastic optimization methods of this kind include simulated annealing (SA), harmony search (HS), particle swarm optimization (PSO), and evolutionary algorithms (e.g., genetic algorithms (GA) and differential evolution). A genetic algorithm (GA) is a stochastic technique that simulates natural evolution in the solution space of the optimization problems. It operates on a population of potential solutions (i.e., individuals) in each iteration (i.e., generation). By combining some individuals of the current population according to predefined operations, a new population that contains better individuals is produced as the next generation. First pioneered by John Holland in the 1960s, genetic algorithms have been widely studied, experimented with, and applied in many fields in the engineering world. The first step of GA is to create randomly an initial population of N_{pop} solutions in the feasible region. GA works on this population and combines (crossover) and modifies (mutation) some chromosomes according to specified genetic operations, to generate a new population with better characteristics. Individuals for reproduction are selected based on their objective function values and the Darwinian principle of the survival of the fittest. The genetic algorithm stochastic optimization method is shown in the supplementary file page 2.

3.3.3 Analysis of kinetic model

Kinetic modeling was used to represent the n-heptane isomerization over each prepared catalyst. The developed new kinetic model contained 16 components lumps and 43 reactions. Each of these components underwent several

reactions according to the proposed kinetic model. Eqs. 4 and 5 were solved using the 4th order Runge-Kutaa integration method to predict the model results, while the genetic algorithm optimization method was used to estimate the optimum kinetic parameters. All programs were written using MATLAB software version 2015a, in which ode45 & GA commands used numerical integration and stochastic optimization, respectively. Three experiments at different temperatures (i.e., 225, 250 and 275^oC) were used to predict the reaction kinetic parameters. The predicted kinetic parameters are presented in **Table 4**, and the composition of the experimental hydroisomerization products and simulated hydroisomerization processes are listed in **Table 5**.

The following observations can be drawn from this table: These results confirm the proposed mechanism by which paraffin isomerization proceeds through an olefin intermediate, with the rate-controlling step being the reaction of the olefin on the acidic sites according to the bifunctional isomerization mechanism [53].



The calculations of the predicted mole fractions compared with the experimental data are good approximate values and were employed to confirm the validity of the proposed reaction mechanism and the reactions kinetic models used to describe 43 reaction paths. The results of the quantity of uncondensed gases in the three experiments at three different temperatures showed that the quantity of these gases increased with increasing temperature, making the path of cracking occur at a higher probability as the high heat broke the hydrocarbons chains. The same results were calculated by the simulation, confirming the validity of the experimental results and the kinetics models that were used. It was found that the olefin mole fractions produced in some experiments were larger than that of the predicted values, which can ascribed to the low flow rate of hydrogen in hydroisomerization rig in the experiment. Some of the differences between the experimental and predicted values, especially in the concentrations of nC₇ and iC₇ were probably caused by operator errors or from the inaccurate measuring items of the hydroisomerization rig. **Table 5** shows the experimental and predicted results plotted in **Fig. 8**, which represent a comparison between the experimental and predicted mol percentages of the products for the three experiments individually. In addition, **Fig. 9** represents these comparisons in one graph. The kinetic model represented the experimental data in moderately acceptable manner. The mean relative error was 23%, which is considered moderate because the input data represents a wide range of operating variables. The level of predicted errors was moderate due to the following points: (1) human and machine errors associated with the experimental work can also affect the kinetic model results; (2) additional cracking reactions may also occur during the initial start-up and final shutdown of the reactor; and (3) in data regression operations, increasing the range of input data and variables will increase the produced error, therefore decreasing the number of datasets will extremely decrease the produced error, but this will be on account of model validity. Therefore, the proposed kinetic model is valid for the experimental data within the operating condition ranges presented in the experimental work.

Table 4. Calculated reactions kinetics parameters

Reaction Number	K (225 °C)	K (250 °C)	K (275 °C)	Ko (mol/ g _{cat} h)	E (j/mol)
1	5.3E-05	0.000126	0.000275	3655.377	74751.9
2	6.83E-05	0.000171	0.000395	15223.55	79608.2
3	3.39E-10	2.11E-09	1.11E-08	14503796	158609.0
4	4.32E-08	2.28E-07	1.03E-06	55152659	144055.7
5	6.46E-10	3.44E-09	1.57E-08	1023610	144952.5
6	8.99E-09	5.15E-08	2.52E-07	65628499	151280.9
7	1.94E-08	9.72E-08	4.19E-07	8210555	139478.0
8	7.59E-09	4.52E-08	2.29E-07	1.28E+08	154760.9
9	0.000159	0.000512	0.001485	7012173	101516.0
10	1.07E-11	5.84E-11	2.74E-10	30075.95	147336.0
11	2.01E-09	1.27E-08	6.74E-08	1.04E+08	159378.0
12	8.26E-05	0.0002	0.000446	8864.7042	76585.5
13	0.00041	0.000771	0.001368	222.82729	54690.5
14	9.76E-13	6.14E-12	3.27E-11	50874.12	159422.1
15	2.01E-10	1.35E-09	7.6E-09	40706154	165049.9
16	4.13E-11	2.6E-10	1.39E-09	2206933.2	159521.7
17	9.29E-12	5.64E-11	2.9E-10	225510.18	156256.9
18	3.09E-05	0.000124	0.00044	138154795	120642.0
19	9.55E-10	5.31E-09	2.52E-08	3660730.3	148611.4
20	1.06E-06	5.57E-06	2.52E-05	1.291E+09	143868.6
21	0.010034	0.020226	0.038245	23553.56	60752.6
22	0.000163	0.00049	0.001336	1721703.4	95599.2
23	0.014797	0.029479	0.055152	27184.756	59737.7
24	2.85E-09	1.99E-08	1.16E-07	1.272E+09	168310.5
25	7.92E-12	4.6E-11	2.27E-10	76736.749	152454.4
26	7.170133	10.9421	16.06679	49771.822	36633.8
27	3.402241	5.032365	7.182437	12283.786	33926.5
28	0.032706	0.070637	0.142213	325419.77	66734.2
29	0.027147	0.055131	0.104955	74498.698	61399.7
30	5.3E-09	3.02E-08	1.47E-07	34152529	150760.2
31	3.69E-08	1.28E-07	3.99E-07	7879.5438	108039.3
32	0.065204	0.160215	0.362678	9648137.1	77914.3
33	0.015321	0.038863	0.090556	4412624.1	80672.6
34	0.003814	0.007656	0.014422	8201.8668	60389.7
35	0.221825	0.358995	0.556026	5262.2875	41723.5
36	1.23E-09	6.87E-09	3.28E-08	5487966.5	149249.5
37	4.32E-10	2.58E-09	1.31E-08	7522841.8	154879.7
38	0.000517	0.00182	0.00571	140281718	109032.7
39	1.1E-05	4.82E-05	0.000185	317763503	128381.2
40	33.4258	46.38633	62.47662	31770.536	28398.9
41	0.049101	0.086722	0.145425	7255.9273	49299.6
42	0.024793	0.043864	0.073669	3796.0962	49446.5
43	11.65437	17.41636	25.09063	52169.596	34816.8

Table 5. Predicted and experimental mole fractions of products, mol%

	Experimental	Mole	Fractions	Predicted	Mole	Fractions
	225°C	250°C	275°C	225°C	250°C	275°C
C ₁	<i>In the experiments</i>			0.003882	0.008079	0.018299
C ₂	<i>total (C₁-C₃) quantities</i>			0.016044	0.032587	0.056989
C ₃	<i>were measured</i>			0.058072	0.098178	0.146424
C ₁ -C ₃	0.0727	0.0912	0.2234	0.077998	0.138844	0.221712
iC ₄	0.0422	0.0631	0.0826	0.038305	0.063098	0.086529
nC ₄	0.0223	0.0234	0.0813	0.018163	0.029005	0.038667
C ₄ =	0.0012	0.0013	0.0106	0.000729	0.0013	0.001917
iC ₅	0.0103	0.0239	0.0392	0.01027	0.02108	0.035226
nC ₅	0.0045	0.0086	0.0157	0.004503	0.008317	0.015701
C ₅ =	0.0013	0.0029	0.0106	0.001272	0.00319	0.006061
iC ₆	0.0042	0.006	0.0079	0.001416	0.00229	0.003293
nC ₆	0.0036	0.0015	0.0104	0.00106	0.0015	0.001966
C ₆ =	0.001	0.0019	0.0033	0.000967	0.0019	0.003377
iC ₇	0.5557	0.609	0.4071	0.644413	0.564472	0.458543
nC ₇	0.2796	0.165	0.0985	0.199449	0.162806	0.124062
C ₇ =	0.0014	0.0022	0.0094	0.001453	0.002199	0.002946

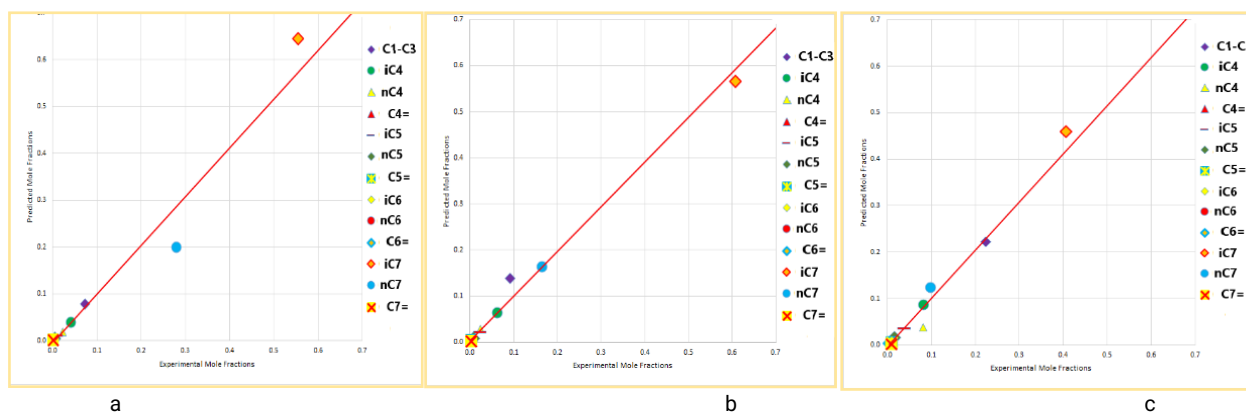


Fig. 8. Predicted mole fractions compared with the experimental data of the hydroisomerization of n-heptane at 1 Mpa, (a) at 225°C, (b) at 250°C, and (c) at 275°C.

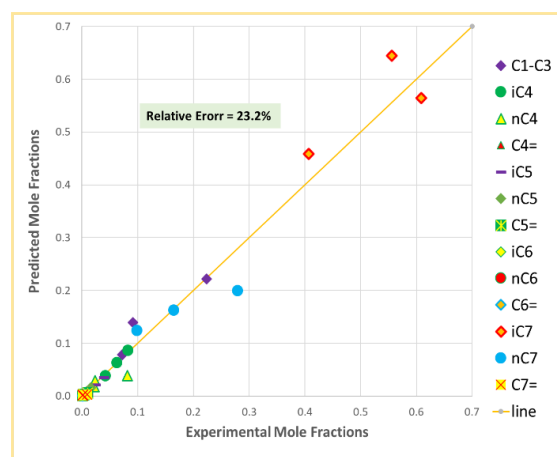


Fig. 9. Predicted mole fractions compared with experimental mole fractions of the hydroisomerization of n-heptane for the three experiments.

Table 6. Calculated average activation energy for n-heptane

Reaction Group	Calculated Average Activation Energy (KJ/mol)
i-paraffin cracking with hydrogen	138.1
n-paraffin cracking	131.6
Olefin hydrogenation to normal paraffin	105.2
n-paraffin dehydrogenation	99.5
paraffin isomerization	84.3
i-paraffin dehydrogenation	83.0
Olefin hydrogenation to iso-paraffins	44.5

Table 6 illustrates the average activation energies for all reaction groups. Lower activation energies were recognized for olefin hydrogenation to iso-paraffins at about 44.5 KJ/mol, while higher activation energies for i-paraffin cracking with hydrogen were about 138.1 KJ/mol. The results of different other works that calculated the activation energies of the hydroisomerization of n-heptane by various catalysts, including those based on Pt metal-loaded zeolite, showed that there is a convergence between the values of the activation energies of hydroisomerization with that calculated in this work when the catalysts utilized were zeolite-based as was used here; for example, the literature [62,63] showed values of 75.7 and 94 kJ/mol, respectively, compared with the activation energy calculated in this work of 84.3kJ/mol. However the calculated activation energies deviated greatly

from this work when the catalysts used were other than zeolite-based catalysts, such as in [64, 65], in which they used Pt/WO₃-ZrO₂ and Pd/Sapo-11, respectively, to obtain activation energies of 114.2 and 115 kJ/mol, respectively.

4. Conclusions

Synthesis of the HY-zeolite have been successfully achieved by hydrothermal and calcination processes. The BET surface area was 481.9 m²/g and the bulk Si/Al ratio was 2.2. A decrease in the surface area was observed after metal was loaded onto the catalyst surface because the metal atoms might have closed some of the zeolite pores. A decrease in zeolite crystallization was also detected in the acidic metal-loaded form of Y-zeolite catalysts due to the fact that metals can act as impurities and can also cause X-ray deflection and lower peak intensities. This can occur due to the calcination of the ammonium form of Y-zeolite at 450°C and then the reduction of metals under hydrogen flow rate at 350°C during the preparation processes, which may cause a partial collapse of the Y-lattice. It was found that the activity of zeolite as a catalyst decreased rapidly if it was not loaded with a noble metal, such as platinum. With the industrial demand for Pt increasing greatly in recent decades, its price has grown exponentially. In this study, a group of Y-zeolite catalysts was manufactured, including three bimetallic catalysts loaded with Pt and Zr metals in different ratios to find a partial replacement for Pt metal. It was found that adding a small and specific percentage of Zr metal can enhance the Lewis acidity in the HY-zeolite framework and contribute to increasing the selectivity of isomers. The Zr metal can also reduce the high Brønsted acidity of zeolite, which increases the rate of hydrocracking reactions at the expense of hydroisomerization reactions and increases the formation of harmful coke, which reduces the life of the catalyst. The use of the Pt-Zr metal combinations led to a higher catalytic activity and a higher yield of total C7 isomers. This improvement was due to a better balance and homogenous relationship between the catalytic functions, which managed to reduce the required amount of the expensive Pt metal. It was partially replaced by the cheap Zr metal, as this study was able to synthesize a competitive bimetallic Cat-9 catalyst consisting of (0.5 wt% Pt + 0.5 wt% Zr)/HY-zeolite, which achieved a higher activity and selectivity than that of the expensive catalyst (1 wt% Pt)/HY-zeolite. The Cat-9 catalyst exhibited the best spectrum distribution for the products of the heptane hydroisomerization process. Thus, it can be selected as the optimal bimetallic catalyst, having achieved the highest yield of isomers at 70.2 %, along with 82.61% and 84.98% for

conversion and selectivity, respectively. In addition, it has been demonstrated during this research that a small amount of Pt (as low as 0.25 wt% with 0.5 wt% Zr loaded on HY-zeolite) can be used as an active and selective hydroisomerization catalyst instead of using a 0.5% Pt/HY-zeolite catalyst alone in order to make the hydroisomerization process more economical. Furthermore, the use of different temperatures during the reaction showed that the conversion of n-heptane to the products increased with increasing reaction temperatures, and the selectivity of the isomers decreased slightly from 86.07% at 225°C to 84.98 % at 250°C. However, it decreased sharply at 275°C, falling to 60.14%, which makes the range of 225-250°C more suitable for the hydroisomerization process under a pressure of 1 MPa because it gives high selectivity. The yield curve had a maximum point near 250°C, realizing the highest yield of 70.2%, and the yield decreased before and after this point, but it decreased significantly at temperatures higher than 250°C. In addition, the hydroisomerization reaction kinetic model was achieved, giving good predicted results in agreement with the experimental calculations with a relative error of no more than 23.2%, based on a computerized simulation that predicted the hydroisomerization reaction paths. It was found that lower activation energies were recognized for n-paraffin hydroisomerization to iso-paraffins (about 84.3 kJ/mol) and olefin hydrogenation to iso-paraffins (about 44.5 kJ/mol), while higher activation energies were found for i-paraffin cracking with hydrogen (about 138.1 kJ/mol). The use of zeolite-based catalysts, especially the bimetallic type loaded with two different metals, mainly Pt and Zr, appears promising in the application of the enhanced production of high-octane fuels containing branched hydrocarbons from light naphtha.

Supporting Information

Supplementary material associated with this article can be found in the online version.

Author Contributions

Younus H. Khalaf: Conceptualization, investigation, resources, writing, review and editing. Bashir Y. Sherhan Al-Zaidi: Methodology, writing, review, and investigation. Zaidoon M. Shakour: Methodology, statistical Analysis, and resources.

References and Notes

- [1] Okuhara, T. *Jpn. Pet. Inst.* **2004**, *47*, 1. [\[Crossref\]](#)
- [2] Available from: <http://blogs.law.columbia.edu/climatechange>. Access October, 2021.
- [3] Mills, G. A.; Heinemann, H.; Milliken, T. H.; Oblad, A. G. *Ind. Eng. Chem.* **1953**, *45*, 134. [\[Crossref\]](#)
- [4] Ono, Y. *Catal. Today* **2003**, *81*, 3. [\[Crossref\]](#)
- [5] Weisz, P. B., In: *Advances in Catalysis*. Eley, D. D.; Selwood, P. W.; Weisz, P. B.; Balandin, A. A.; De Boer, J. H.; Debye, P. J.; Emmett, P. H.; Horiuti, J.; Jost, W.; Natta, G.; Rideal, E. K.; Taylor, H. S., eds. Academic Press, 1962.
- [6] Saito, M.; Iwasaki, T. *Bull. Jpn. Pet. Inst.* **1976**, *18*, 117. [\[Crossref\]](#)
- [7] Degnan, T. F. *Top. Catal.* **2000**, *13*, 349. [\[Crossref\]](#)
- [8] Pariente, J. P.; Sánchez-Sánchez, M.; *Structure and Reactivity of Metals in Zeolite Materials*, 178th ed. Cham: Springer, 2018.
- [9] Gates, B. C.; Flytzani-Stephanopoulos, M.; Dixon, D. A.; Katz, A. *Catal. Sci. Technol.* **2017**, *7*, 4259. [\[Crossref\]](#)
- [10] Liu, J. *ACS Catal.* **2017**, *7*, 34. [\[Crossref\]](#)
- [11] Corma, A.; Nemeth, L. T.; Renz, M.; Valencia, S. *Nature* **2001**, *412*, 423. [\[Crossref\]](#)
- [12] Corma, A.; Llabrés i Xamena, F. X.; Prestipino, C.; Renz, M.; Valencia, S. *J. Phys. Chem. C* **2009**, *113*, 11306. [\[Crossref\]](#)
- [13] Zhu, Y.; Chuah, G.; Jaenicke, S. *J. Catal.* **2004**, *227*, 1. [\[Crossref\]](#)
- [14] Lewis, J. D.; Van de Vyver, S.; Román-Leshkov, Y. *Angew. Chem., Int. Ed* **2015**, *54*, 9835. [\[Crossref\]](#)
- [15] Moliner, M.; Corma, A. *Microporous Mesoporous Mater.* **2014**, *189*, 31. [\[Crossref\]](#)
- [16] Corma, A.; Iborra, S.; Velty, A. *Chem. Rev.* **2007**, *107*, 2411. [\[Crossref\]](#)
- [17] Román-Leshkov, Y.; Davis, M. E. *ACS Catal.* **2011**, *1*, 1566. [\[Crossref\]](#)
- [18] Moliner, M. *Dalton Trans.* **2014**, *43*, 4197. [\[Crossref\]](#)
- [19] Luo, H. Y.; Lewis, J. D.; Román-Leshkov, Y. *Annu. Rev. Chem. Biomol. Eng.* **2016**, *7*, 663. [\[Crossref\]](#)
- [20] Yan, G. X.; Wang, A. Q.; Wachs, I. E.; Baltrusaitis, J. *Appl. Catal., A* **2019**, *572*, 210. [\[Crossref\]](#)
- [21] Li, H.; Wang, J.; Zhou, D.; Tian, D.; Shi, C.; Müller, U.; Feyen, M.; Gies, H.; Xiao, F.-S.; De Vos, D.; Yokoi, T.; Bao, X.; Zhang, W. *Microporous Mesoporous Mater.* **2015**, *218*, 160. [\[Crossref\]](#)
- [22] Sinfelt, J. H. *Acc. Chem. Res.* **1987**, *20*, 134. [\[Crossref\]](#)
- [23] Sinfelt, J. H. *Annu. Rev. Mater. Sci.* **1972**, *2*, 641. [\[Crossref\]](#)
- [24] Sinfelt, J. H., In: *Metal-Metal Bonds and Clusters in Chemistry and Catalysis*. Fackler, J. P., Ed. Springer, Boston, MA, 1990.
- [25] Yang, L.; Song, Z.; Yu, Y.; Zhu, L.; Xia, D. *Catal. Surv. Asia* **2020**, *24*, 104. [\[Crossref\]](#)
- [26] Kitaev, L. E.; Bukina, Z. M.; Yushchenko, V. V.; Nesterenko, N. S.; Alekseenko, L. N. *Pet. Chem.* **2006**, *46*, 246. [\[Crossref\]](#)
- [27] Jarvis, J. S.; Harrhy, J. H.; He, P.; Wang, A.; Liu, L.; Song, H. *Chem. Commun.* **2019**, *55*, 3355. [\[Crossref\]](#)
- [28] Lin, C.; Pan, H.; Yang, Z.; Han, X.; Tian, P.; Li, P.; Xiao, Z.; Xu, J.; Han, Y.-F. *Ind. Eng. Chem. Res.* **2020**, *59*, 6424. [\[Crossref\]](#)
- [29] Al-Zaidi, B. Y. S. The effect of modification techniques on the performance of zeolite-Y catalysts in hydrocarbon cracking reactions. [Master's thesis] Manchester, United Kingdom: Department of Chemical Engineering, University of Manchester, 2011. [\[Link\]](#)
- [30] Warner, T. E.; Galsgaard Klokke, M.; Nielsen, U. G. *J. Chem. Educ.* **2017**, *94*, 781. [\[Crossref\]](#)
- [31] Chu, P. *J. Catal.* **1976**, *43*, 346. [\[Crossref\]](#)
- [32] Kitaev, L. E.; Bukina, Z. M.; Yushchenko, V. V.;

- Nesterenko, N. S. *Pet. Chem.* **2006**, *46*, 398. [\[Crossref\]](#)
- [33] Liu, P.; Yao, Y.; Zhang, X.; Wang, J. *Chin. J. Chem. Eng.* **2011**, *19*, 278. [\[Crossref\]](#)
- [34] Tan, Y.; Hu, W.; Du, Y.; Li, J. *Appl. Catal. A* **2021**, *611*, 117916. [\[Crossref\]](#)
- [35] Lyu, Y.; Zhan, W.; Wang, X.; Yu, Z.; Liu, X.; Yan, Z. *Fuel* **2020**, *274*, 117855. [\[Crossref\]](#)
- [36] Wang, S.; Cao, M.; Sun, S.; Jiang, H.; Duan, Y.; Kong, X.; Wang, H. *Fuel* **2020**, *280*, 118274. [\[Crossref\]](#)
- [37] Huang, C.; Han, D.; Guan, L.; Zhu, L.; Mei, Y.; He, D.; Zu, Y. *Fuel* **2022**, *307*, 121790. [\[Crossref\]](#)
- [38] Meynen, V.; Cool, P.; Vansant, E. F. *Microporous Mesoporous Mater.* **2009**, *125*, 170. [\[Crossref\]](#)
- [39] Baerlocher, C.; McCusker, L. B.; Olson, D. H., Atlas of Zeolite Framework Types, Sixth ed. Amsterdam, Netherlands: Elsevier, 2007.
- [40] Ma, H.; Zhang, J.; Wang, M.; Sun, S. *ChemistrySelect* **2019**, *4*, 7981. [\[Crossref\]](#)
- [41] Matti, A. H.; Surchi, K. M. *International Journal of Innovative Research in Science, Engineering and Technology* **2014**, *3*, 2319.
- [42] Souza, M. J. B.; Silva, A. O. S.; Fernandes Jr, V. J.; Araujo, A. S. *React. Kinet. Catal. Lett.* **2003**, *79*, 257. [\[Crossref\]](#)
- [43] Nsaif, M.; Abdulhaq, A.; Farhan, A.; Neamat, S. *Journal of Asian Scientific Research* **2012**, *2*, 927.
- [44] Chester, A. W.; Derouane, E. G.; Zeolite Characterization and Catalysis, 11th ed. Dordrecht: Springer, 2009.
- [45] Tolstoy, V.; Altangerel, B. *Mater. Lett.* **2007**, *61*, 123. [\[Crossref\]](#)
- [46] Qian, Z.; Shi, J. L. *Nanostruct. Mater.* **1998**, *10*, 235. [\[Crossref\]](#)
- [47] Allen, A. D.; Theophanides, T. *Can. J. Chem.* **1964**, *42*, 1551. [\[Crossref\]](#)
- [48] Johnstone, T. C.; Lippard, S. J. *JBIC, J. Biol. Inorg. Chem.* **2014**, *19*, 667. [\[Crossref\]](#)
- [49] Chen, Z.; Wang, H.; Wang, X.; Chen, P.; Liu, Y.; Zhao, H.; Zhao, Y.; Duan, Y. *Sci. Rep.* **2017**, *7*, 40061. [\[Crossref\]](#)
- [50] Benesi, H.; Curtis, R.; Studer, H. *J. Catal.* **1968**, *10*, 328. [\[Crossref\]](#)
- [51] Shkurenok, V. A.; Smolikov, M. D.; Yablokova, S. S.; Kir'yanov, D. I.; Paukshtis, E. A.; Koscheev, S. V.; Gulyaeva, T. I.; Belyi, A. S. *Procedia Eng.* **2016**, *152*, 94. [\[Crossref\]](#)
- [52] Ribeiro, F. R., In: Zeolites: Science and Technology. Ribeiro, F. R.; Rodrigues, A. E.; Rollmann, L. D.; Naccache, C., eds. Dordrecht: Springer, 1984, chapter 20.
- [53] Sinfelt, J. H.; Hurwitz, H. L.; Rohrer, J. C. *J. Phys. Chem.* **1960**, *64*, 892. [\[Crossref\]](#)
- [54] Ribeiro, F.; Marcilly, C.; Guisnet, M. *J. Catal.* **1982**, *78*, 267. [\[Crossref\]](#)
- [55] Potter, M. E.; Le Brocq, J. J.; Oakley, A. E.; McShane, E. B.; Vandegehuchte, B. D.; Raja, R. *Catalysts* **2020**, *10*, 1099. [\[Crossref\]](#)
- [56] Kooh, A. B.; Han, W.-J.; Hicks, R. F. *Catal. Lett.* **1993**, *18*, 209. [\[Crossref\]](#)
- [57] Wang, Z.; Kamo, A.; Yoneda, T.; Komatsu, T.; Yashima, T. *Appl. Catal., A* **1997**, *159*, 119. [\[Crossref\]](#)
- [58] Alvarez, F.; Giannetto, G.; Guisnet, M.; Perot, G. *Appl. Catal.* **1987**, *34*, 353. [\[Crossref\]](#)
- [59] Meusinger, J.; Corma, A. *J. Catal.* **1995**, *152*, 189. [\[Crossref\]](#)
- [60] Shakor, Z. M.; AbdulRazak, A. A.; Sukkar, K. A. *Arabian J. Sci. Eng.* **2020**, *45*, 7361. [\[Crossref\]](#)
- [61] Śliwińska, A.; Smolinski, A.; Kucharski, P. *Appl. Sci.* **2019**, *9*, 4705. [\[Crossref\]](#)
- [62] Denayer, J. F. M.; Martens, J. A.; Jacobs, P. A.; Thybaut, J. W.; Marin, G. B.; Baron, G. V. *Appl. Catal., A* **2003**, *246*, 17. [\[Crossref\]](#)
- [63] Saberi, M. A.; Le Van Mao, R. *Appl. Catal., A* **2003**, *242*, 139. [\[Crossref\]](#)
- [64] Khurshid, M.; Al-Khattaf, S. S. *Appl. Catal., A* **2009**, *368*, 56. [\[Crossref\]](#)
- [65] Höchtel, M.; Jentys, A.; Vinek, H. *J. Catal.* **2000**, *190*, 419. [\[Crossref\]](#)

How to cite this article

Khalaf, Y. H.; Al-Zaidi, B. Y. S.; Shakour, Z. M. *Orbital: Electron. J. Chem.* **2022**, *14*, 153. DOI: <http://dx.doi.org/10.17807/orbital.v14i3.17429>